energies

MDPI

Article

Grid Code-Dependent Frequency Control Optimization in Multi-Terminal DC Networks

Melanie Hoffmann [1,†], Harold R. Chamorro [2,*,†], Marc René Lotz [3], José M. Maestre [2], Kumars Rouzbehi [2], Francisco Gonzalez-Longatt [4], Michael Kurrat [1], Lazaro Alvarado-Barrios [5] and Vijay K. Sood [6]

1 Institute for High Voltage Technology and Power Systems, Braunschweig University of Technology, 2, 38106 Braunschweig, Germany; melanie.hoffmann@tu-braunschweig.de (M.H.); m.kurrat@tu-braunschweig.de (M.K.)
2 Departamento de Ingeniería de Sistemas y Automatica, Universidad de Sevilla, 4, 41004 Seville, Spain; pepemaestre@us.es (J.M.M.); krouzbehi@us.es (K.R.)
3 Institute of Electrical Systems and Automation Technology (IfEA), Ostfalia University of Applied Sciences, 38302 Wolfenbüttel, Germany; m.lotz@ostfalia.de
4 Francisco Gonzalez-Longatt is with Electrical Power Engineering, University of South-Eastern Norway, 40, 3679 Notodden, Norway; fglongatt@fglongatt.org
5 Departamento de Ingeniería, Universidad Loyola Andalucía, 4, 41004 Seville, Spain; lalvarado@uloyola.es
6 Electrical, Computer and Software Engineering, Ontario Tech University, Oshawa, ON L1H 7K4, Canada; vijay.sood@uoit.ca
* Correspondence: hr.chamo@ieee.org
† These authors contributed equally to this work.

Received: 6 October 2020; Accepted: 3 December 2020; Published: 8 December 2020

Abstract: The increasing deployment of wind power is reducing inertia in power systems. High-voltage direct current (HVDC) technology can help to improve the stability of AC areas in which a frequency response is required. Moreover, multi-terminal DC (MTDC) networks can be optimized to distribute active power to several AC areas by droop control setting schemes that adjust converter control parameters. To this end, in this paper, particle swarm optimization (PSO) is used to improve the primary frequency response in AC areas considering several grid limitations and constraints. The frequency control uses an optimization process that minimizes the frequency nadir and the settling time in the primary frequency response. Secondly, another layer is proposed for the redistribution of active power among several AC areas, if required, without reserving wind power capacity. This method takes advantage of the MTDC topology and considers the grid code limitations at the same time. Two scenarios are defined to provide grid code-compliant frequency control.

Keywords: MTDC; frequency control; fast frequency control; low-inertia; wind power; grid code; non-synchronous generation; python-PSCAD-interface; particle swarm optimization

1. Introduction

Power transmission infrastructure is experiencing continuous evolution around the globe due to the large-scale deployment of renewable energy sources and the need for new technologies that guarantee reliable and smart operation. The integration of renewables has been promoted by governmental agencies and environmental policies to combat global warming while efficiently upgrading power grids [1]. Consequently, inertia levels may decrease in the future due to the large integration of wind power, with an impact on the power system dynamics [2], including the frequency response of conventional alternating current (AC) systems [3].

High-voltage direct current (HVDC) and multi-terminal direct current (MTDC) networks, composed of multiple voltage source converters (VSC), play a key role in the interconnection of AC grids and renewable power integration. For instance, in the United States, the Western Electric Coordination Council (WECC) and their Transmission System Operators (TSO) are working on these HVDC installations and envision the use of so-called super-grids to prepare the system for further offshore wind capacity [4], minimize resistive losses [5], transmit power over long distances [6] and bring potential services to the AC counterparts [7]. Moreover, the very fast active power frequency support capability of the high-capacity VSC–HVDC systems is expected to be implemented in future to connect the three North America power grids—i.e., the Eastern Interconnection (EI), the WECC and the Texas Interconnection (ERCOT)—to improve the frequency performance in the three interconnections after contingencies [8,9].

Similarly, China envisions the use of a HVDC network that interconnects several AC areas in order to protect them in case of natural disasters and guarantee a high reliability in the connected sub-areas [10]. Other examples for HVDC installations can be found in Korea, where islands should be connected using a zero-carbon subsystem, and in Australia, where hydro power and islands should be connected. The goal of these projects is to reduce the cost–distance of installation and maintenance prices [11,12]. In Europe, it is expected that an MTDC connection will be implemented in the future to interconnect the different TSOs, such as the North Sea Region, which interconnects the Netherlands, Germany and Denmark [13].

The beneficial partnership of HVDC and AC grids can exploit the flexibility and controllability of MTDC technology to improve and counteract the impact of inertia reduction by providing fast frequency control support [14]. By adding supplementary controllers to the VSCs, it is possible to improve the primary frequency control and inject power into areas in which it is needed [15].

In order to address the decreasing inertia levels, several authors have proposed innovative techniques to improve the frequency control through MTDC networks [16]; e.g., by means of multi-agent distributed control [17], by using model predictive control (MPC) for frequency regulation [18], and by using inertia emulation control for HVDC point-to-point connections [19,20] specifying the amount of permissible DC voltage variation versus the inertia provided. A similar approach is presented in [20], in which the authors used the same concept but in MTDC networks. The influence of overlaid MTDC networks on the connected AC networks and the grid code compliance is studied in [21], where the coordination concern is emphasized.

A communication-free adaptive coordinated control strategy to allow both offshore wind farms (OWFs) and VSC–HVDC to contribute to the frequency regulation in the onshore AC grid is presented in [22]. By means of this approach, the frequency extremes and the rate of change of frequency (RoCoF) in the on-shore grid are reduced. An scheme that is activated upon the detection of a significant frequency deviation with a support limit requested from other AC systems interconnected by VSCs is proposed in [23]. An auxiliary dead-band controller for fast-frequency support in MTDC is proposed in [24], which uses measurements of RoCoF and frequency deviation to modify the dead-band set-point of fast-frequency controllers.

A control approach for VSC stations in an MTDC grid to provide mutual frequency support among asynchronous AC networks is developed in [25]. This control system modifies the active power references of each droop-controlled converter considering its adjacent AC systems to enable frequency support. A similar frequency control strategy for VSC-based MTDC systems is proposed in [26] to facilitate the exchange of primary frequency reserves among asynchronous AC systems. This strategy employs a frequency control method that utilizes a reference signal calculated from global measurements, which reflects the overall frequency dynamics of all connected asynchronous AC systems [26]. Another coordinated control scheme that gives priority to a frequency versus active power droop fitted to onshore VSCs is proposed in [27] and used to control the operation of MTDC systems during multiple power imbalances on AC grids. A frequency-coordinated control (FCC) strategy based on situation awareness is proposed in [28] and makes full use of the frequency

regulation potential of wind turbines and HVDC transmission. Another communication-free control scheme that can allocate frequency support power between onshore VSC stations using local frequency signal during frequency events is shown in [29].

Several optimization applications have been used in MTDC networks. For instance, particle swarm optimization (PSO) has been employed in [30] for the DC voltage controller loops in an MTDC network. A distributed MPC is applied in [31] as an enhancer of automatic generation control (AGC) in MTDC networks. An optimization problem has been formulated in [32] to improve the nadir and RoCoF considering offshore grids and several contingencies. A supervisory power re-scheduler scheme using MPC is presented in [33], which helps the DC network to satisfy limits even under terminal outages. Another application of the PSO and MTDC networks is presented in [34], where the inner and outer controllers are optimized to enhance the voltage performance.

Primary frequency control enhancement requires innovative solutions that address the limitations in the system and provide adequate responses that maintain the stability of the system and guarantee that the controllers are between their narrow margins [35]. Therefore, the motivation of this paper is the development of an optimization approach for the maximization of the power injection and minimization of the nadir and RoCoF. A frequency control optimization algorithm is proposed in this paper to improve the frequency control support in AC grids through fast-frequency HVDC support. Before designing this control concept, grid code requirements need to be analyzed and—if needed—extended or adjusted. In this regard, this work presents an assessment of the forecoming European HVDC development, showing the limitations and possible results of optimizing frequency control through the PSO method. The objective of this paper is to propose a practical solution for frequency control optimization to ensure the grid code compliance of HVDC-connected systems. The main focus of this research is to find a procedure that can be used in reality to improve the behavior of an AC system connected to a HVDC converter. The PSO optimization methodology has been chosen as one example of an optimization method.

The rest of this article is organized as follows. Section 2 gives an overview of the current situation regarding the frequency grid code requirements in Europe, emphasizing the under-frequency limits and the synthetic inertia requirements. Section 3 explains the theoretical frameworks of frequency control and the MTDC system dynamics. The proposed methods are introduced in Section 4. The simulation results and discussions are presented in Section 5. Finally, Section 6 concludes the paper.

2. Frequency Related Grid Code Requirements

2.1. Regulation Levels

Different regulation levels can be identified in the case of HVDC connections. For example, Figure 1 shows the relation of three different grid connection requirement levels for some European countries; namely, European, national and TSO-specific requirement levels.

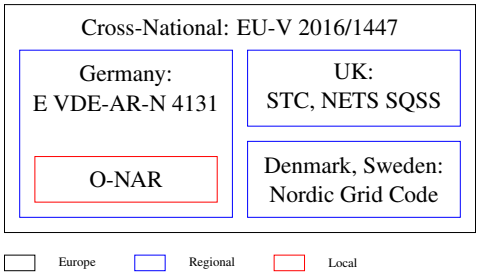

Figure 1. Grid code levels.

The European Commission regulation 2016/1447 [36] has set the legal framework for the HVDC connections of OWFs in the European Union (EU). In [37], harmonized rules are provided to set a clear legal framework for grid connections. These rules should ensure EU-wide electricity trade possibilities,

system security, the integration of renewable electricity sources, increased competition and a more efficient use of the grid and energy sources for the benefit of society in the EU [36].

The EU legislation needs to be adjusted in each country for specific regional requirements. For example, this has been realized in Germany by creating the Technical Connection Rules for HVDC Systems and HVDC-Connected Power Plants [38], which has the purpose of forming the basis for the safe application of new technologies in existing systems; e.g, integrating offshore wind energy with the lowest possible losses. The objective of the German grid code is that HVDC systems can provide ancillary services [38]. The contents of other national grid codes—e.g., from the UK, Denmark and Sweden—are comparable with the German grid code.

Finally, national-level grid codes are often transferred to grid connection rules that are applicable for certain grid operators [39]. In Germany, for example, the grid operator TenneT created the grid connection rules for OWFs that are connected to their existing grid [40]. These grid operator-specific requirements usually match the regional requirements.

2.2. Requirements for Power Plants Connected to HVDC Systems

The defined 10 s average frequency in the offshore AC grid needs to be within specific limits around a nominal frequency of 50 Hz. For HVDC connections, the following requirements need to be fulfilled:

- 50 Hz $\pm$ 2% (49 Hz to 51 Hz) for 95% of the week;
- 50 Hz $\pm$ 15% (42.5 to 57.5 Hz) 100% of the time.

The grid codes also define the frequency-dependent power supply. OWFs have to feed active power without limitations into the grid within a frequency range of 49.0 Hz to 50.2 Hz. It is permitted to limit the active power in-feed when the frequency goes below 49 Hz. The maximum active power reduction is 2% of the maximum generator power per Hz (see Figure 2). The maximum allowed active power reduction when under this frequency is defined by the the reference power of the OWF and not by the momentarily available power.

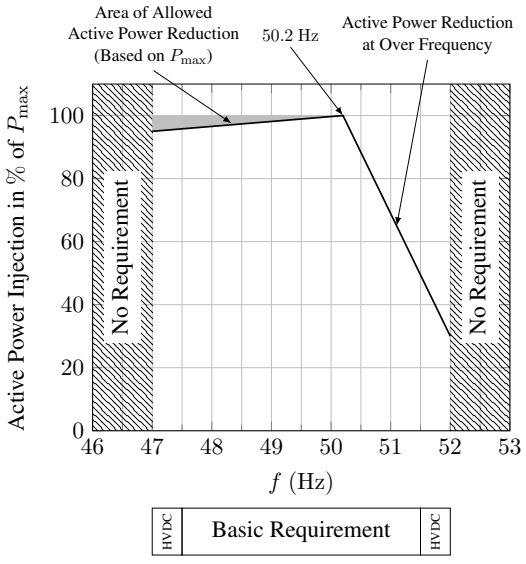

Figure 2. Requirements for the frequency-dependent power supply of generators connected via HVDC systems (based on [40]).

An additional requirement for power plants connected to a HVDC system is to provide a synthetic flywheel mass to limit the frequency gradient in the case of under and/or over-frequency. Details need to be defined with the responsible TSO [38]. As shown in Figure 2, an extended frequency range is

required for HVDC connections. Usually, the offshore VSC operates in U/f control mode, which means that the voltage and the frequency are controlled at the offshore AC side.

The European Network of Transmission System Operators for Electricity (ENTSO-E) states in [41] that the pre and post-fault conditions for the RoCoF need to be specified regarding the minimum short-circuit capacity at the connection point pre and post-fault, as well as the active and reactive power operating point of the power generating module and the voltage at the connection point pre-fault. In order to harmonize European requirements, power-generating modules need to remain connected to the grid at a frequency of or below the following moving averages: ±2 Hz for 500 ms, ±1.5 Hz for 1000 ms and ±1.25 Hz for 2000 ms.

2.3. Synthetic Inertia

The aim of requiring synthetic inertia, according to the EU Network code [36], is to replace the effect of the inertia of traditional synchronous power-generating modules by a power park module or HVDC system. Synthetic inertia is stated in Article 14 of [36] as a requirement that can be specified by the relevant TSO. In a later published guidance document from the ENTSO-E, the need for synthetic inertia is discussed in more detail [42]. It is specified in [36] and in Table 1 that, in the case of a frequency step, the initial activation of the active power frequency response should not exceed 2 s ($t_{1,\text{inertia}}$). This activation time can be shorter for power-generating modules without inertia ($t_{1,\text{no inertia}}$), which would apply, for example, to renewable energy generators unless justified otherwise. The maximum admissible delay time of full activation is defined as t_2 (see Table 1), unless longer activation times are allowed by the relevant TSO for reasons of system stability. The full active power frequency response should be available for up to 15 to 30 min. The exact duration is also specified by the relevant TSO.

Figure 3 illustrates the active power frequency response capability curve. On the x-axis is the time in seconds and on the y-axis is ΔP divided by P_{max}, where ΔP is the change in active power output from the power-generating module, such as a wind turbine generator (WTG), and P_{max} stands for the maximum active power capacity of the generating module. The times t_1 and t_2 are the initial delay time and the time for full activation, respectively.

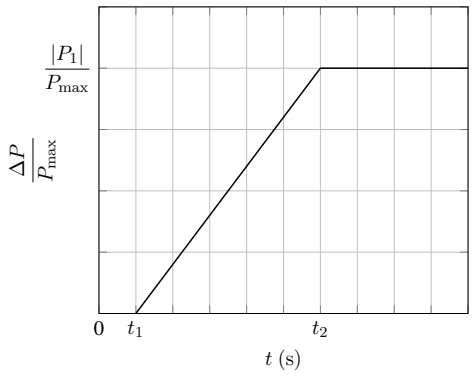

Figure 3. Constant DC voltage control.

Table 1 defines the ranges of the parameters of the active power frequency response. The values are chosen to ensure stabilization (primary frequency control) and restoration to the nominal frequency (secondary frequency response). These preconditions can then help to maintain the power exchange flows between control areas to the scheduled values.

Table 1. Active power frequency response parameters. TSO: Transmission System Operators.

Parameter	Value Range
$\frac{\lvert\Delta P_1\rvert}{P_{max}}$	1.5–10%
$t_{1,\text{inertia}}$	2 s
$t_{1,\text{no inertia}}$	TSO
t_2	30 s

The requirement of providing synthetic inertia and therefore supporting the AC grid is also specified in the draft of the German grid connection code [38]. This additional requirement for HVDC systems consists of the ability to provide synthetic inertia in case of frequency deviations. This control should be activated at over or under-frequency by a fast adjustment of the active power supplied to/from the AC grid to limit the frequency gradient. The basic parameters of this control system will be discussed between the grid operator and the owner of the connected generation system.

2.4. Requirements from Grid Codes

This subsection gives a short overview of the grid code requirements, especially for a frequency-dependent power supply and synthetic inertia control. The content is defined in a more general way in the European HVDC network code [36]. These general requirements are specified in a next step in each country to take national specific conditions into account. Apart from technical grid code requirements, such as the RoCoF or details about how long an HVDC converter needs to be able to stay connected, more regulations and boundary conditions are defined for HVDC networks. For example, the component limits, such as the maximum Insulated-Gate Bipolar Transistor (IGBT) current-carrying capacity or the cable capacities, need to be considered. Furthermore, the simulation model needs to be built so that very small simulation time steps, in the range of milliseconds, can be used. This is necessary because frequency changes appear within very short time frames.

3. HVDC Modeling

Let a power system be described as a graph $\mathcal{G} = \{\mathcal{V}, \mathcal{E}\}$ where $\mathcal{V}$ is the set of vertices modeling the n_b buses of the system and $\mathcal{E}$ is the set of edges, which represents all n_l branches of the system [43]. We consider this power system to be an MTDC transmission network consisting of n converters, where each converter is connected to an AC system, denoted as $i \in \{1, \ldots, n\}$ [44]. The converters are interconnected by the MTDC network.

3.1. AC System Dynamics

The AC dynamics of subsystem i are represented by an aggregated model given by the swing equation,

$$M_i \dot{\omega}_i = P_i^m - P_i^e + P_i^c, \tag{1}$$

where $M_i \in \mathbb{R} > 0$ is the inertia constant, ω_i is the AC frequency of the system, P_i^m and P_i^e are the mechanical and electrical power, respectively, and P_i^c is the power injected from the converter into the grid. Note that the active power of the converter P_i^c is considered positive when power is injected positively into the AC system.

The governor model is given by

$$\dot{P}_i^m = \frac{1}{T_i^a}\left(K_i^R \omega_i - T_i^c K_i^R \dot{\omega}_i - P_i^m\right), \tag{2}$$

where $T^a \in \mathbb{R}> 0$ is the governor time constant, $T^c \in \mathbb{R}> 0$ is the governor phase constant and $K^R \in \mathbb{R}> 0$ is the droop constant. The secondary control loop is neglected here, as this document is focused on primary control only.

3.2. Converter and MTDC System Dynamics

For the nodes connected to converter i, averaged models are used, which are characterized by their equivalent DC-side and AC-side equations as follows:

$$C_i \dot{V}_i = - \sum_{\substack{\forall j \in \mathcal{V} \\ j \neq i}} \frac{1}{R_{ij}} \left(V_i - V_j \right) + I_i^{inj} \tag{3}$$

where V_i is the DC voltage of the converter at node i, C_i is the converter equivalent capacitance and I_i^{inj} is the current that is injected from the converter into the node. The HVDC transmission lines, connecting two nodes i and j, are modeled with their resistances R_{ij}.

The injected current will be calculated as follows, based on the notation of [45], with

$$I_i^{inj} = I_i^{inj'} - I_i^{\text{loss}}, \tag{4}$$

$$I_i^{inj'} = \frac{1}{V_i} \sum_{j=1,2,3} v_i^{c,j} i_i^j, \tag{5}$$

$$I_i^{loss} = R_i^{loss} \frac{\left(I_i^{inj} \right)^2}{V_i}. \tag{6}$$

The voltage $v_i^{c,j}$ represents the combination of upper and lower-arm voltages of the converter AC side, while i_i^j is the grid current. The index $j \in \{1, 2, 3\}$ stands for the three phases of the converter AC grid connection. The current I_i^{loss} models converter losses with an equivalent resistance R_i^{loss}.

The AC-side converter dynamics can then be modeled with the combined inductance L_i and resistance R_i of the transformer and the phase reactor, respectively.

$$L_i \frac{\mathrm{d}}{\mathrm{d}t} \left(\frac{I_i^{inj}}{3} - \frac{i_i^j}{2} \right) + R_i \left(\frac{I_i^{inj}}{3} - \frac{i_i^j}{2} \right) = -v_i^j - v_i^{c,j} \tag{7}$$

3.3. Converter Control

A synchronous d-q reference frame approach is conventionally employed to facilitate VSC control [46]. Here, the d-axis aligns with the grid voltages, meaning $d = 1$ and $q = 0$. With the grid current dynamics in the d-q frame,

$$R_i^{dq} i_i^d + L_i^{dq} \dot{i}_i^d = v_i^{c,d} + \omega_i^{dq} L_i^{dq} i_i^q - v_i^d, \tag{8}$$

$$R_i^{dq} i_i^q + L_i^{dq} \dot{i}_i^q = v_i^{c,q} - \omega_i^{dq} L_i^{dq} i_i^d - v_i^q, \tag{9}$$

where R_i^{dq} and L_i^{dq} are the combined resistance and inductance of the transformer and the phase reactor, respectively, and v_i^d and v_i^q are the grid voltages. Linear decoupling and neglecting the resistances give the following terms for the converter voltages:

$$v_i^{c,d} = u_i^{c,d} - L_i^{dq} \omega_i^{dq} i_i^q + v_i^d \tag{10}$$

$$v_i^{c,q} = u_i^{c,q} + L_i^{dq} \omega_i^{dq} i_i^d + v_i^q \tag{11}$$

where $u_i^{c,d}$ and $u_i^{c,q}$ are the control signals which represent the control of the grid currents i_i^d and i_i^q in the *d*-*q* frame. Proportional–integral (PI) controllers are utilized, with the following control laws:

$$u_i^{c,d} = K_i^{P,d} \cdot \left(i_i^{d,ref} - i_i^d \right) + K_i^{I,d} \cdot \int_0^t \left(i_i^{d,ref} - i_i^d \right) \mathrm{d}\tau, \tag{12}$$

$$u_i^{c,q} = K_i^{P,q} \cdot \left(i_i^{q,ref} - i_i^q \right) + K_i^{I,q} \cdot \int_0^t \left(i_i^{q,ref} - i_i^q \right) \mathrm{d}\tau. \tag{13}$$

The current controllers make up the inner control loops. Additionally, active and reactive power controllers are added as the outer control loops, again as PI controllers. With the calculation of active and reactive power,

$$P_i^c = v_i^{c,d} i_i^d, \tag{14}$$

$$Q_i^c = v_i^{c,q} i_i^q, \tag{15}$$

the control laws can be formulated as

$$\begin{aligned} i_i^{d,\mathrm{ref}} &= K_i^{P,P} \cdot \left(P_i^{c,\mathrm{ref}} - P_i^c \right) \\ &+ K_i^{I,P} \cdot \int_0^t \left(P_i^{c,ref} - P_i^c \right) \mathrm{d}\tau \end{aligned} \tag{16}$$

$$\begin{aligned} i_i^{q,\mathrm{ref}} &= K_i^{P,Q} \cdot \left(Q_i^{c,\mathrm{ref}} - Q_i^c \right) \\ &+ K_i^{I,Q} \cdot \int_0^t \left(Q_i^{c,ref} - Q_i^c \right) \mathrm{d}\tau \end{aligned} \tag{17}$$

As can be seen, the outer control loops produce the set points for the inner current control loops.

3.4. Droop Control

In some MTDC grid converters, additional DC voltage droop control is deployed. This proportional control provides a linear relationship between the DC voltage deviation and the active power set points. This droop control characteristic is also implemented in converters 1, 3 and 4 of the MTDC network (Figure 4):

$$P_i^{c,\mathrm{ref}} = P_i^{c,\mathrm{nom}} + K_i^V \cdot \left(V_i^{ref} - V_i \right) \tag{18}$$

The active power nominal reference set point $P_i^{c,\mathrm{nom}}$ will be altered by the droop control output, with K_i^V as the droop constant, to create the active power reference set point P_i^c.

As regards the AC frequency droop control, the following control scheme will be proposed. The nominal *d*-axis current set point $i_i^{d,\mathrm{nom}}$ will be altered by Δi_i^d to obtain the reference.

$$i_i^{d,\mathrm{ref}} = i_i^{d,\mathrm{nom}} + \Delta i_i^d \tag{19}$$

Among the conventional constant droop gains, denoted as $k_i^{\omega_i}$, the frequency derivative will also be considered with

$$RoCoF_i = \dot{\omega}_i, \tag{20}$$

so that the set point alteration results in

$$\Delta i_i^d = RoCoF_i \cdot k_i^{\omega_i} \cdot \left(\omega_i^{ref} - \omega_i \right). \tag{21}$$

Figure 5 shows the overall control principle and system dynamics of the converter and its AC and DC grid connection. In addition, the equations defined above are used in the outer as well as in the inner control loops [47].

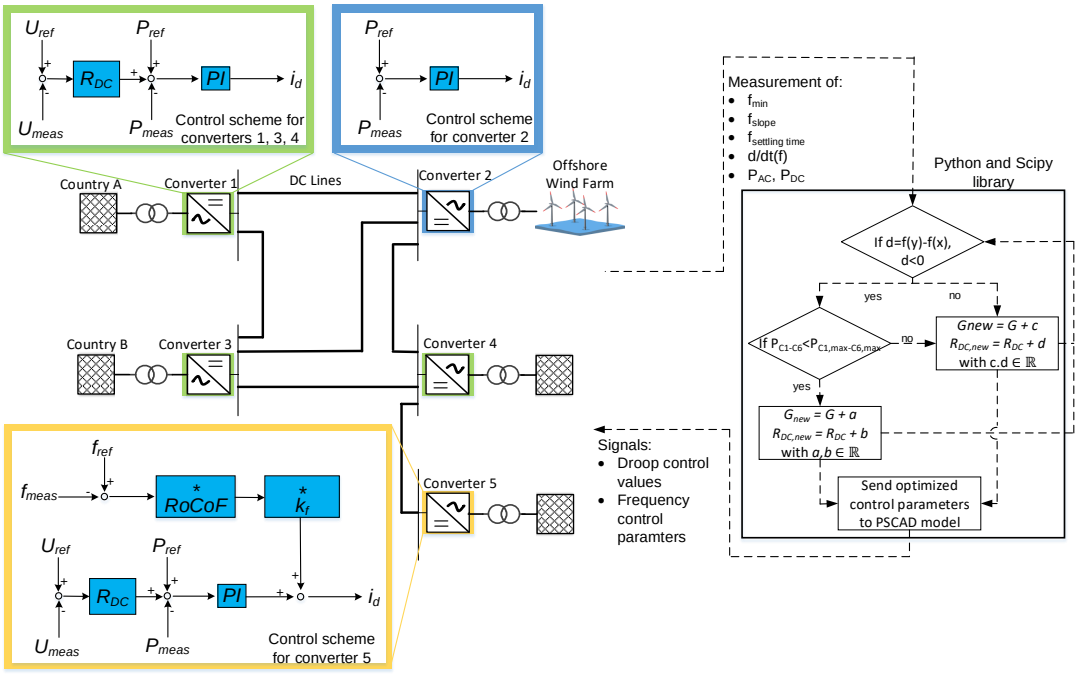

Figure 4. Methodology for the optimization of the AC grid stabilization using a PSCAD and Python interface.

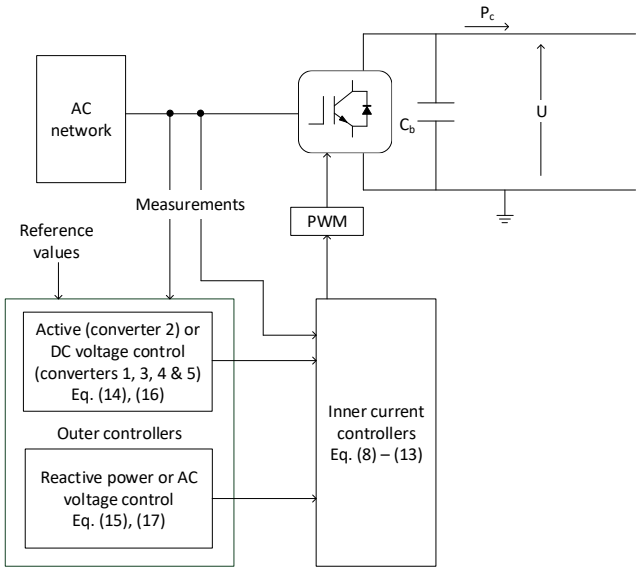

Figure 5. Overall converter control scheme.

3.5. Phase-Locked Loop

The phase-locked loop (PLL) is needed both for the overall converter control and for synchronization during frequency deviations. The algorithm follows a common PI-based control principle, where the set point of the grid voltage q-component is zero.

$$\dot{\theta}_i = K_i^{P,PLL} \cdot \left(v_i^{q,ref} - v_i^q\right) + \int_0^t K_i^{I,PLL} \cdot \left(v_i^{q,ref} - v_i^q\right) \cdot \mathrm{d}\tau \tag{22}$$

where $\dot{\theta}_i$ is the deviation of the reference frame angle at node i, $K_i^{P,PLL}$ and $K_i^{I,PLL}$ are the proportional and integral gain, $v_i^{q,ref}$ us the q-component grid voltage set point, which is zero, and v_i^q the calculated q-component of the grid voltage. The d-q reference frame angle $\theta_i = \omega_i t$ is then expressed by

$$\theta_i = \int_0^t \dot{\theta}_i \cdot \mathrm{d}\tau. \tag{23}$$

It is assumed that the PLL dynamics are negligible compared to the dynamics of the frequency deviations.

4. Proposed Controller

4.1. Optimal Performance Indicators

The optimization problem is formulated using the RoCoF, the nadir and the settling time t_s of the AC system frequency to realize the best possible and most robust solution. Figure 6 shows the four parameters that are utilized to optimize the frequency responses. Each parameter has a specific area in which it needs to be optimized. The RoCoF is the slope when a load event appears, and its gradient should be as low as possible according to grid code requirements (see Section 2) to ensure that the frequency controller has enough time to react. This parameter is therefore optimized in the red area. The nadir is the minimum frequency reached after a load event. This should be as close to the nominal frequency as possible. This parameter is optimized in the blue area. The settling time t_s and the settling time need to be reduced in the yellow and green optimization areas, respectively.

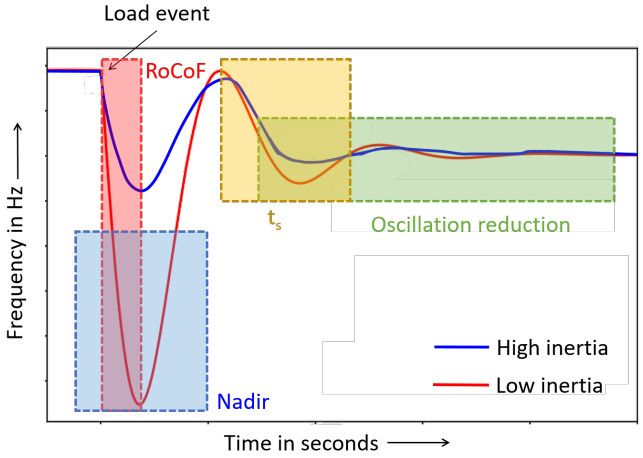

Figure 6. Frequency response areas.

Figure 7 illustrates the theoretical effect of the implemented frequency optimization. The blue trajectory, which represents a high-inertia system, can be developed by optimizing the frequency control regarding the four parameters explained in Figure 6. In contrast, the red graph shows the frequency response without optimization. The frequency responses in Figure 7 are only valid for the primary control, which has the goal of stabilizing the frequency. The secondary control is then responsible for bringing the frequency back to the nominal frequency, illustrated in Figure 7 as a black dashed line.

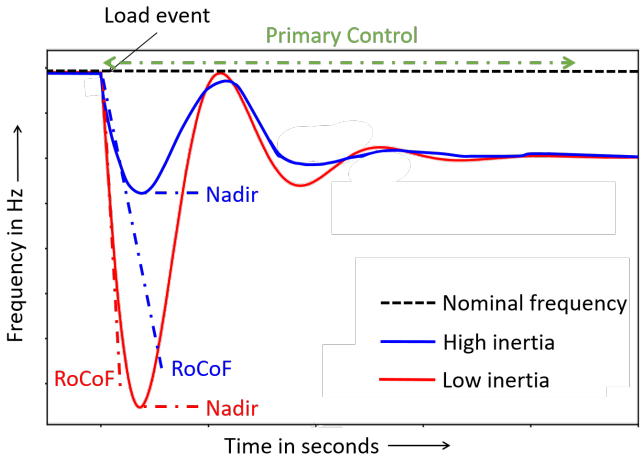

Figure 7. Frequency response with high and low inertia.

A novel, flexible, optimal strategy has been proposed, with the overall flow chart shown in Figure 4.

4.2. Controller Optimization Using Particle Swarm Optimization

Particle swarm optimization (PSO) is a methodology used for the optimization of non-linear systems. The goal is to find the best solution considering the previous solutions for each iteration [48]. The PSO-based optimization problem is formulated below. Equation (24) illustrates the fitness function, which needs to be minimized. This equation consists of three characteristic parameters: the nadir, RoCoF and the settling time t_s.

$$min\ f(w) = v_1 \cdot nadir + v_2 \cdot RoCoF + v_3 \cdot t_s \tag{24}$$

The weights v_1, v_2, and v_3 are assigned and related as follows:

$$v_3 = 1 - v_2 - v_1 \tag{25}$$

where v_1 is from 0 to 0.7 and v_2 is from 0 to 0.3.

4.3. Python-PSCAD Interface

In terms of the optimization procedure, a distinct interface has been utilized. As shown in Figure 4, measurements of specific parameters are given to a Python environment using the PSCAD Automation Library, in which the optimization algorithm is implemented. The resulting output—i.e., the adapted control parameters—are then fed back into the PSCAD to generate the successive input. Then, Python works as an optimization controller that adjusts the frequency controller parameters, controlling the power flow of the considered grid in the most efficient way. The frequency control parameters calculated in the optimization algorithm need to be within certain limits to ensure the practical implementation. For the optimization, different parameters need to be measured in the converters and transferred to the optimization algorithm. For the frequency optimization, it is especially important to obtain the minimum frequency within a certain time frame, as well as the frequency slope and the frequency settling time until a stable frequency value is reached after an event that resulted in a frequency change. The change of frequency over a time step is also important for the optimization algorithm. Similarly, the power flow on the AC as well as on the DC side needs to be measured. From these input values, the optimization algorithm can analyze how the frequency event can be supported by the HVDC converter. Therefore, the result of the algorithm is that droop control values and frequency controller parameters are fed back to the HVDC converter

controller. More precisely, the power should be distributed within the MTDC system to support the AC grid in which the frequency event appeared.

The main challenge of utilizing this interface is to change parameters in the PSCAD model during the simulation. To ensure an appropriate adjustment of the parameters, the simulation needs to be started again after each optimization iteration, which makes the entire optimization process quite time-consuming. It is therefore beneficial to identify the optimal parameter sets for different operation conditions before the commissioning of the system.

5. Results and Discussion

A five-terminal HVDC system was modeled in PSCAD as shown in Figure 4. In general, power can flow in both directions, from the AC grid to the DC grid and vice versa. The basic definition is that converters 1, 3 and 4 work as inverters in a DC droop control mode, and converters 2 and 5 as rectifiers utilizing a constant active power control. Via converter 2, an OWF is connected to the MTDC system. Note that the OWF is modeled as an ideal AC voltage source. The five-terminal HVDC grid consists of the AC part, the DC part and the transmission line part. The AC current voltage from the source flows into the converters and is then converted into DC current voltage by the control system of these converters. After that, it flows through the DC transmission lines into the inverters, where the DC current and voltage are converted back into AC current and voltage. The load event is modeled on the AC side of converter 5, where the AC grid is defined by the swing-governor equation to combine the AC frequency response with the DC power injection. Transmission lines are modeled in PSCAD as being between 80 km and 250 km in length. The DC voltage level was chosen to be 420 kV for this benchmark topology. To examine and optimize the frequency behavior in such a MTDC system, the PSCAD Automation Library was used. This allowed the coupling of PSCAD and Python via an interface in which data could be collected from the model and optimized parameters could be given back to the model. In addition, it allowed the use of the Scipy optimization library in Python.

As shown in Figure 6, different characteristics of the frequency response needed to be considered for the optimization:

- The *RoCoF* should not be very steep according to the grid code requirements. If the *RoCoF* is too steep, the converters would disconnect from the AC grid and could therefore no longer support it, thus provoking power imbalances;
- The *nadir* should not drop below a specific value to ensure that the converter stays connected to the grid and follows the grid code limits;
- The settling time t_s needs to be minimized to reach a stable operating state as quickly as possible, as an earlier recovery means less impact.

To achieve grid code-compliant system behavior in accordance with the three requirements above, different control parameters were adjusted as part of the optimization algorithm; for example, changing the droop control values resulted in a different RoCoF, nadir and settling time.

The optimization procedure was executed for two different scenarios, which were then compared to the base case without additional frequency control. The first scenario focused on optimization using an additional frequency control loop connected in converter 5, as shown in Figure 4. For this first scenario, only $k_i^{\omega_i}$ was used. In the second scenario, the *RoCoF* parameter was also implemented in addition to scenario 1.

5.1. Base Case Scenario

This scenario is defined as the operation of the five-terminal HVDC grid without additional frequency control. This scenario is represented by the first iteration, defined as $w = 0$, in scenarios A and B.

5.2. Scenario A

Scenario A is defined as the case in which only the gain parameter $k_i^{\omega_i}$ is included in the frequency optimization. In order to minimize the fitness function, which is defined by the *RoCoF*, nadir and settling time, different values for $k_i^{\omega_i}$ were calculated with Python and given to the PSCAD model.

The next step was to simulate the frequency event; again, Python was utilized to analyze the results. If the fitness function improved, shown by a lower value, the parameters in PSCAD were accordingly changed in Python. Figure 8 shows the process of optimizing the frequency response in the case of a load event in the AC grids connected to the converters. More specifically, the iteration number is denoted as w.

As shown in Figure 8, the nadir and the settling time were mainly optimized. The RoCoF was also a key parameter, but optimizing the gain value of the frequency controller did not have a large effect on the frequency response. In addition, it can be seen that the grid code requirements regarding the allowed frequency band and the settling time were met.

Figure 8 shows that the frequency derivative changed in a very steep way in the case of a load event in the AC grid connected to converter 5. This effect can be used for the optimization of the frequency controller and make it react faster. This will be evaluated in scenario B.

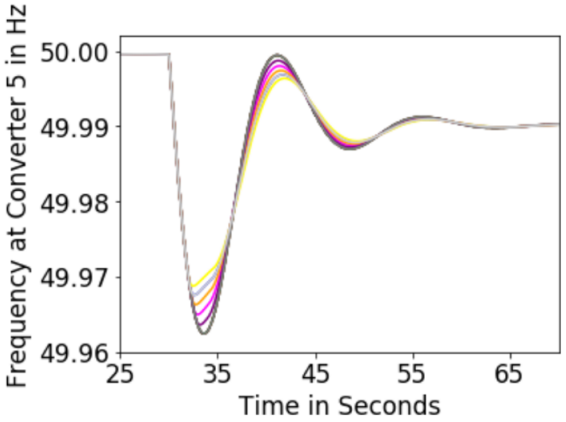

(**a**) Frequency optimization scenario A.

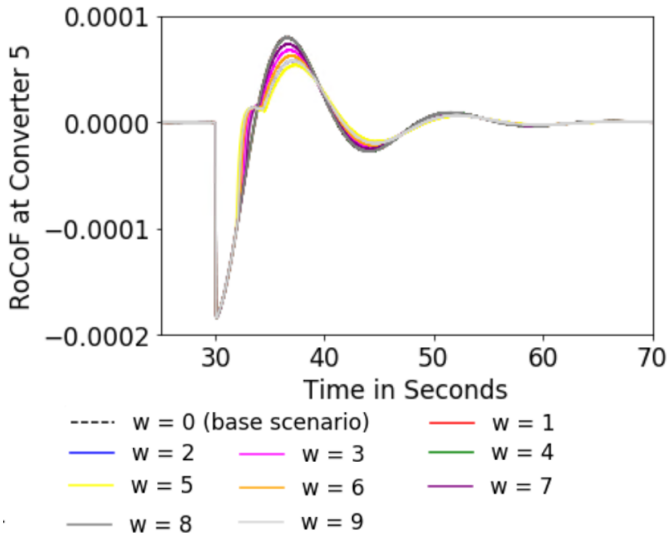

(**b**) DC power at converter 1.

Figure 8. Frequency derivative/rate of change of frequency (RoCoF) scenario A.

Figure 9 shows the change of the active power supplied from AC grids 1 and 2. The activation time was defined by the grid codes (see Table 1) at around 2 s, which was the allowed activation time delay for systems with inertia. Therefore, it was possible to change a system without inertia to respond similarly to a system with inertia.

It can be seen that the power could support the frequency stabilization in AC grid 5. Therefore, the MTDC topology was part of the frequency controller optimization. In this scenario, neither large batteries nor a reserve from the OWFs were needed. With these figures, it becomes clear that the MTDC grid needs to support the AC grid more as more frequency response is requested by the frequency controller.

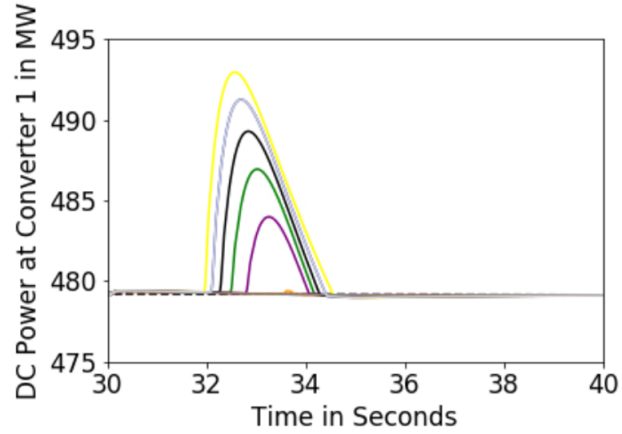

(**a**) DC Power at Converter 1.

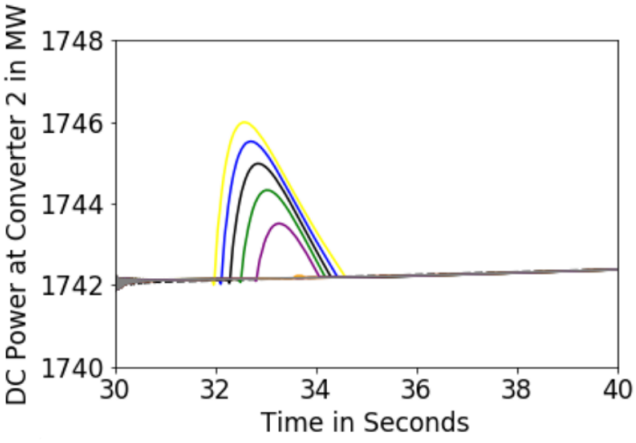

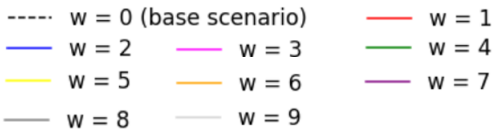

(**b**) DC Power at Converter 2.

Figure 9. DC Power.

Table 2 provides the settling time in seconds and the nadir in Hz for each iteration w. The settling time together with the nadir is an important parameter that allows the derivation of the behavior of the HVDC system. Consequently, it can be used to improve the developed optimization algorithm. Table 2 shows that the optimization algorithm searches for the global optimum by varying the important control parameters in different directions. This is also depicted in the settling time. The nadir improves with each iteration from 49.9624 Hz to 49.9697 Hz. This is a marginal improvement but shows the principle function of the proposed algorithm. To consider existing grid codes and the stability of the

overall system, certain limits had to be considered in the optimization process, which led to rather small changes.

Table 2. Settling time and nadir development during the optimization process.

Iteration w	Settling Time (s)	Nadir (Hz)
w = 1	58.7967	49.9624
w = 2	59.0327	49.9630
w = 3	58.8410	49.9636
w = 4	58.8014	49.9642
w = 5	59.1660	49.9658
w = 6	58.9222	49.9663
w = 7	58.8060	49.9676
w = 8	59.3174	49.9688
w = 9	59.0327	49.9697

5.3. Scenario B

Like scenario A, scenario B also took the frequency derivative into account. The frequency derivative, as shown in Figures 8 and 10, shows a fast reaction in the case of a frequency change. This characteristic makes it very suitable for controller optimization.

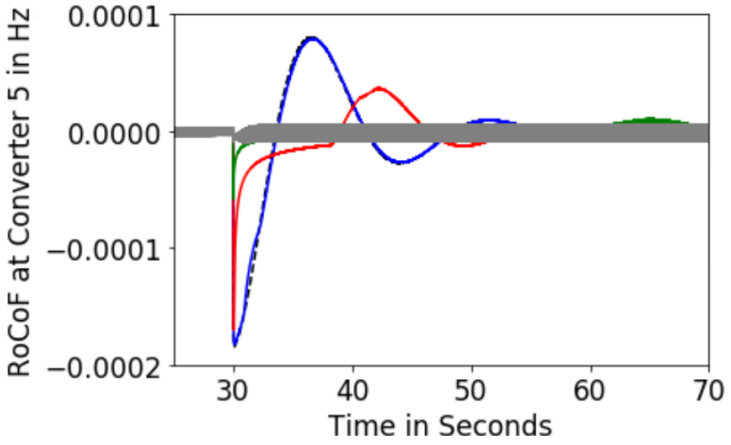

(**a**) Frequency derivative.

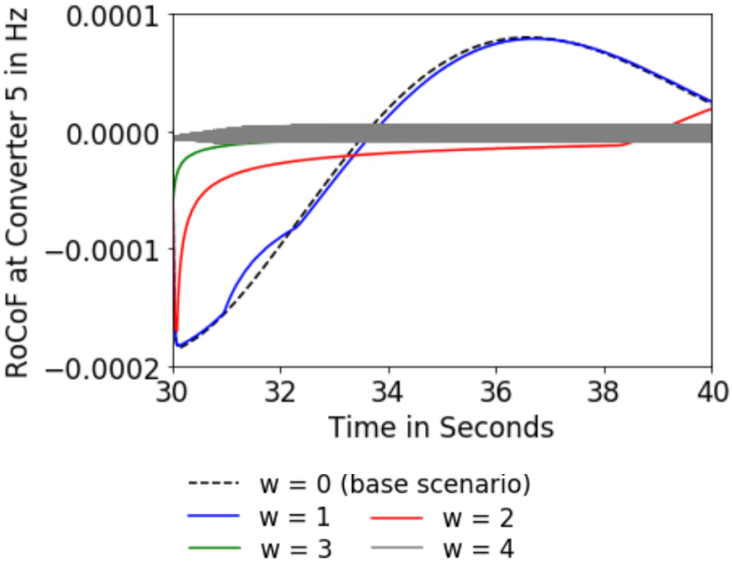

(**b**) Frequency derivative zoom.

Figure 10. Frequency derivative/RoCoF scenario B.

Figure 11 shows how the derivative can improve the frequency response after a load event. The derivative can be multiplied with a constant parameter to increase its influence. Figure 11 illustrates that the RoCoF, the nadir and the settling time are influenced by the derivative. The larger the constant multiplied with the RoCoF, the greater the influence of this. Comparing Figures 11 and 8, it can be seen that the derivative influences the nadir as well as the RoCoF and the settling time, whereas the impact of the frequency control without the derivative only improves the nadir.

Figure 11 also shows that the nonlinear behavior of the frequency grows with the product of the constant and the derivative. Increasing this constant by a factor of 10 from w = 1 to w = 2 results in a lower effect than that of the difference between w = 2 to w = 3 as shown in Figure 11b.

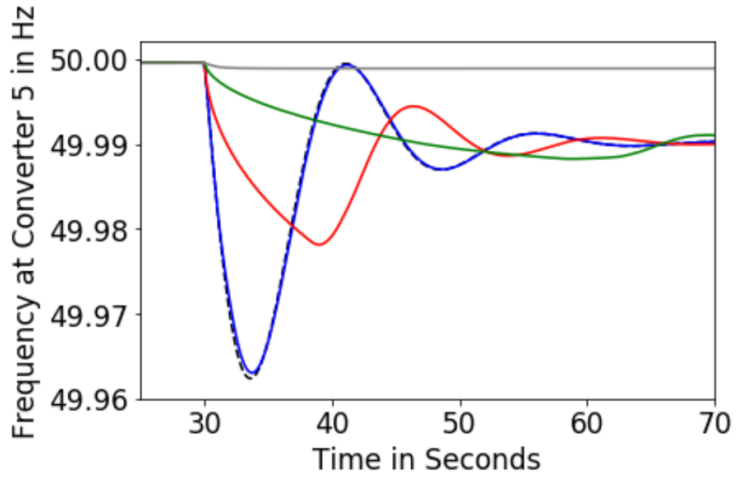

(**a**) Frequency–time response.

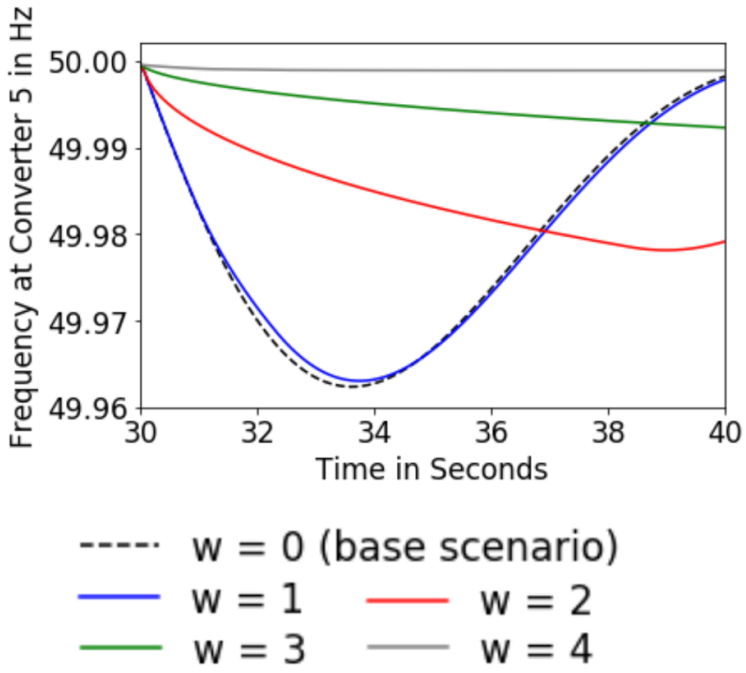

(**b**) Frequency–time response zoom.

Figure 11. Time response scenario B.

The RoCoF remains equal for scenario A, as well as scenario B, between the grid code limits as defined in Section 2. It is important to ensure this by adding these boundary conditions to the constraints of the optimization problem.

Figure 10 shows the frequency derivative behind the frequency graphs in Figure 11. It can be seen that multiplying the frequency derivative results in a steeper curve when the constant is higher. The iteration w = 4 illustrated in grey illustrates that the derivative can also lead to unstable and negative behavior if the constant multiplied with the derivative was chosen to be too high. Therefore, constraints need to be defined for the optimization of the frequency control, and these constraints should also be included in grid codes.

Figure 12a,b shows the active power at converter 1 and 2, respectively, for the different values of optimization. These figures show that, in general, the power change is similar for power levels around 500 MW and 1750 MW. The negative effect of an overly high constant multiplied with the derivative is also visible in Figure 12. Iteration w = 4 shows this and illustrates how the power supplied from the AC grids would change over a longer time and more drastically at the time of the load event. Comparing scenario B with scenario A, it becomes visible that the frequency control also has an effect on the power supplied to converter 5, at which the frequency event occurred. The power adjustments in the other converters occurred much faster compared to the case without the RoCoF being used.

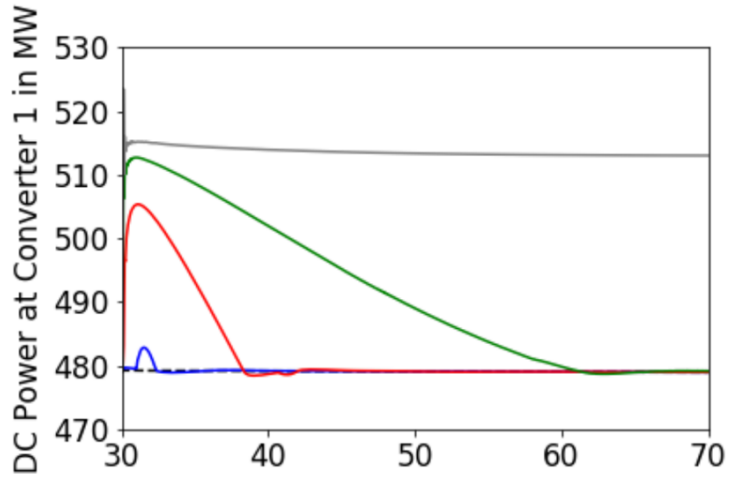

(**a**) DC power at converter 1.

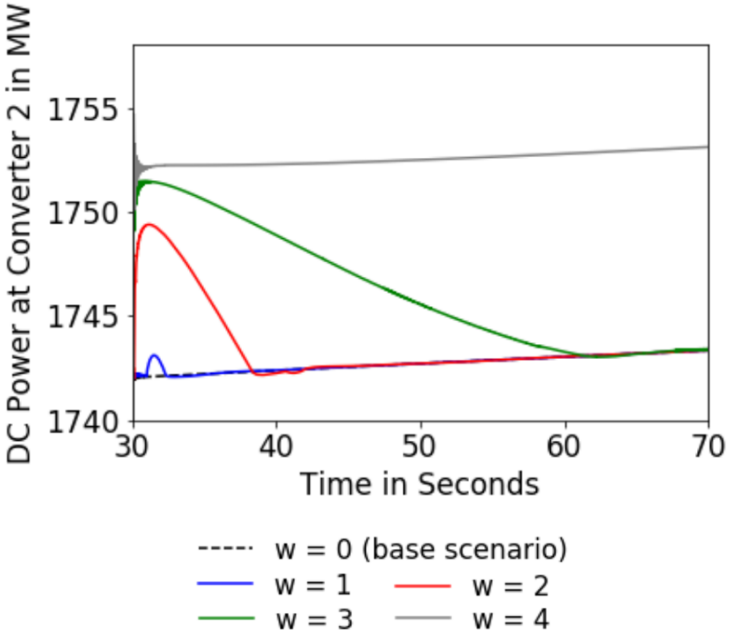

(**b**) DC power at converter 2.

Figure 12. Active power response scenario B.

6. Conclusions

In this paper, a novel approach for the optimization of frequency response has been presented. Simulations using PSCAD and Python interfaces have been used to illustrate the proposed method. The simulation model represents a low-inertia system with HVDC converter stations with additional frequency control. The special focus of this paper relied on the use of a specific topology for optimized frequency response. Consequently, no large storage capacities or OWF reserves were needed. This can improve the economic capability significantly. Another focus of this research was the grid code requirements; however, it can also be seen that grid code requirements are not yet sufficiently specific and that only some rules are defined on the national levels by the various TSOs. This paper can be seen as a first step-by-step guide to propose a method to transform low-inertia systems into a network that behaves similarly to one with inertia. The necessary steps to be taken to transform low-inertia networks using an optimization technique were presented. In addition, the most relevant parameters for the network transformation as well as for the adjustment of the network code were identified. One parameter that was investigated in detail was the frequency derivative for controller optimization, since it can have negative effects on the frequency support. Additionally, the importance of converters in case of low-inertia grids was demonstrated. Finally, it was possible to generalize the process, based on frequency control optimization, for the transformation of a low-inertia system into a network that behaves similarly to one with inertia. In future research, focus will be placed on defining different parameters with more precise values so that they can be included in future network codes. Furthermore, additional optimization techniques will be applied for the analysis.

Author Contributions: Conceptualization, M.H. and H.R.C.; methodology, M.H., H.R.C., and M.R.L.; software, M.H.; validation, M.H., H.R.C., and M.R.L.; formal analysis, J.M.M.; investigation, M.H., H.R.C.; resources, M.K.; data curation, M.H.; writing—original draft preparation, M.H., H.R.C., M.R.L., J.M.M., F.G.-L., and V.K.S.; writing—review and editing, K.R., J.M.M., V.K.S., and F.G.-L.; visualization, H.R.C., M.H.; supervision, M.K., J.M.M., and project administration, M.K.; funding acquisition, L.A.-B. All authors have read and agreed to the published version of the manuscript.

Funding: This work was supported in part by the Laboratorio de Simulación Hardware-in-the-loop para Sistemas Ciberfísicos under Grant TEC2016-80242-P (AEI/FEDER), in part by the Spanish Ministry of Economy and Competitiveness under Grant DPI2016-75294-C2-2-R.

Conflicts of Interest: The authors declare no conflict of interest.

References

1. Strbac, G.; Konstantinidis, C.V.; Moreno, R.; Konstantelos, I.; Papadaskalopoulos, D. It's All About Grids: The Importance of Transmission Pricing and Investment Coordination in Integrating Renewables. *IEEE Power Energy Mag.* **2015**, *13*, 61–75. doi:10.1109/MPE.2015.2418075.
2. Chamorro, H.R.; Ordonez, C.A.; Peng, J.C.; Ghandhari, M. Non-synchronous generation impact on power systems coherency. *IET Gener. Trans. Distrib.* **2016**, *10*, 2443–2453. doi:10.1049/iet-gtd.2015.1233.
3. Milano, F.; Dörfler, F.; Hug, G.; Hill, D.J.; Verbič, G. Foundations and Challenges of Low-Inertia Systems (Invited Paper). In Proceedings of the 2018 Power Systems Computation Conference (PSCC), Dublin, Ireland, 11–15 June 2018; pp. 1–25. doi:10.23919/PSCC.2018.8450880.
4. Liu, X.; Lindemann, A. Control of VSC-HVDC Connected Offshore Windfarms for Providing Synthetic Inertia. *IEEE J. Emerg. Select. Top. Power Electr.* **2018**, *6*, 1407–1417. doi:10.1109/JESTPE.2017.2751541.
5. Cao, J.; Du, W.; Wang, H.F.; Bu, S.Q. Minimization of Transmission Loss in Meshed AC/DC Grids with VSC-MTDC Networks. *IEEE Trans. Power Syst.* **2013**, *28*, 3047–3055. doi:10.1109/TPWRS.2013.2241086.
6. Ordonez, C.A.; Puentes, A.; Chamorro, H.R.; Ramos, G. *p-q* theory for active compensation applied to supergrids and microgrids. In Proceedings of the 2012 Workshop on Engineering Applications, Bogota, Colombia, 2–4 May 2012; pp. 1–6. doi:10.1109/WEA.2012.6220088.

7. Chamorro, H.R.; Ramos, G. Harmonic and power flow hybrid controller applied to VSC based HVDC stations. In Proceedings of the 2010 IEEE/PES Transmission and Distribution Conference and Exposition: Latin America (T D-LA), Sao Paulo, Brazil, 8–10 November 2010; pp. 245–250. doi:10.1109/TDC-LA.2010.5762889.
8. Litzenberger, W.; Mitsch, K.; Bhuiyan, M. When It's Time to Upgrade: HVdc and FACTS Renovation in the Western Power System. *IEEE Power Energy Mag.* **2016**, *14*, 32–41. doi:10.1109/MPE.2015.2501178.
9. Yuan, Z.; You, S.; Liu, Y.; Liu, Y.; Osborn, D.; Pan, J. Frequency control capability of Vsc-Hvdc for large power systems. In Proceedings of the 2017 IEEE Power Energy Society General Meeting, Birmingham, UK, 10–12 February 2017; pp. 1–5.
10. Zhou, H.; Su, Y.; Chen, Y.; Ma, Q.; Mo, W. The China Southern Power Grid: Solutions to Operation Risks and Planning Challenges. *IEEE Power Energy Mag.* **2016**, *14*, 72–78. doi:10.1109/MPE.2016.2547283.
11. Gemmell, B.; Korytowski, M. Refurbishments in Australasia: Upgrades of HVdc in New Zealand and FACTS in Australia. *IEEE Power Energy Mag.* **2016**, *14*, 72–79. doi:10.1109/MPE.2015.2501106.
12. Kim, S.; Kim, H.; Lee, H.; Lee, J.; Lee, B.; Jang, G.; Lan, X.; Kim, T.; Jeon, D.; Kim, Y.; et al. Expanding Power Systems in the Republic of Korea: Feasibility Studies and Future Challenges. *IEEE Power Energy Mag.* **2019**, *17*, 61–72. doi:10.1109/MPE.2019.2896690.
13. Irnawan, R.; da Silva, F.F.; Bak, C.L.; Bregnhøj, T.C. An initial topology of multi-terminal HVDC transmission system in Europe: A case study of the North-Sea region. In Proceedings of the 2016 IEEE International Energy Conference (ENERGYCON), Leuven, Belgium, 4–8 April 2016; pp. 1–6. doi:10.1109/ENERGYCON.2016.7513880.
14. Pan, J.; Callavik, M.; Lundberg, P.; Zhang, L. A Subtransmission Metropolitan Power Grid: Using High-Voltage dc for Enhancement and Modernization. *IEEE Power Energy Mag.* **2019**, *17*, 94–102. doi:10.1109/MPE.2019.2896691.
15. Chamorro, H.R.; Riaño, I.; Gerndt, R.; Zelinka, I.; Gonzalez-Longatt, F.; Sood, V.K. Synthetic Inertia Control Based on Fuzzy Adaptive Differential Evolution. *Int. J. Electr. Power Energy Syst.* **2019**, *105*, 803–813. doi:10.1016/j.ijepes.2018.09.009.
16. Zhang, W.; Rouzbehi, K.; Luna, A.; Gharehpetian, G.B.; Rodriguez, P. Multi-terminal HVDC grids with inertia mimicry capability. *IET Renew. Power Gener.* **2016**, *10*, 752–760. doi:10.1049/iet-rpg.2015.0463.
17. Andreasson, M.; Dimarogonas, D.V.; Sandberg, H.; Johansson, K.H. Distributed Controllers for Multiterminal HVDC Transmission Systems. *IEEE Trans. Control Netw. Syst.* **2017**, *4*, 564–574. doi:10.1109/TCNS.2016.2535105.
18. McNamara, P.; Milano, F. Model Predictive Control-Based AGC for Multi-Terminal HVDC-Connected AC grids. *IEEE Trans. Power Syst.* **2018**, *33*, 1036–1048. doi:10.1109/TPWRS.2017.2694768.
19. Zhu, J.; Booth, C.D.; Adam, G.P.; Roscoe, A.J.; Bright, C.G. Inertia Emulation Control Strategy for VSC-HVDC Transmission Systems. *IEEE Trans. Power Syst.* **2013**, *28*, 1277–1287. doi:10.1109/TPWRS.2012.2213101.
20. Zhu, J.; Guerrero, J.M.; Hung, W.; Booth, C.D.; Adam, G.P. Generic inertia emulation controller for multi-terminal voltage-source-converter high voltage direct current systems. *IET Renew. Power Gener.* **2014**, *8*, 740–748. doi:10.1049/iet-rpg.2014.0109.
21. Ndreko, M.; Bucurenciu, A.; Popov, M.; van der Meijden, M.A.M.M. On grid code compliance of offshore mtdc grids: modeling and analysis. In Proceedings of the 2015 IEEE Eindhoven PowerTech, Eindhoven, The Netherlands, 29 June–2 July 2015; pp. 1–6. doi:10.1109/PTC.2015.7232398.
22. Ye, Y.; Lu, Z.; Xie, L.; Qiao, Y. A Coordinated Frequency Regulation Strategy for VSC-HVDC Integrated Offshore Wind Farms. In Proceedings of the 2018 IEEE Power Energy Society General Meeting (PESGM), Portland, OR, USA, 5–10 August 2018; pp. 1–5.
23. Papangelis, L.; Guillaud, X.; Cutsem, T.V. Frequency support among asynchronous AC systems through VSCs emulating power plants. In Proceedings of the 11th IET International Conference on AC and DC Power Transmission, Birmingham, UK, 10–12 February 2015; pp. 1–9.
24. Jose, K.; Adeuyi, O.; Liang, J.; Ugalde-Loo, C.E. Coordination of fast frequency support from multi-terminal HVDC grids. In Proceedings of the 2018 IEEE International Energy Conference (ENERGYCON), Limassol, Cyprus, 3–7 June 2018; pp. 1–6.
25. Kirakosyan, A.; El-Saadany, E.F.; El Moursi, M.S.; Salama, M. Selective Frequency Support Approach for MTDC Systems Integrating Wind Generation. *IEEE Trans. Power Syst.* **2020**, doi:10.1109/TPWRS.2020.3006832.

26. Zhang, Q.; McCalley, J.D.; Ajjarapu, V.; Renedo, J.; Elizondo, M.; Tbaileh, A.; Mohan, N. Primary Frequency Support through North American Continental HVDC Interconnections with VSC-MTDC Systems. *IEEE Trans. Power Syst.* **2020**, doi:10.1109/TPWRS.2020.3013638.
27. Adeuyi, O.D.; Cheah-Mane, M.; Liang, J.; Jenkins, N. Fast Frequency Response From Offshore Multiterminal VSC–HVDC Schemes. *IEEE Trans. Power Deliv.* **2017**, *32*, 2442–2452.
28. Ai, Q.; Liu, T.; Yin, Y.; Tao, Y. Frequency coordinated control strategy of HVDC sending system with wind power based on situation awareness. *IET Gener. Trans. Distrib.* **2020**, *14*, 3179–3186.
29. Xiong, Y.; Yao, W.; Wen, J.; Lin, S.; Ai, X.; Fang, J.; Wen, J.; Cheng, S. Two-Level Combined Control Scheme of VSC-MTDC Integrated Offshore Wind Farms for Onshore System Frequency Support. *IEEE Trans. Power Syst.* **2020**, doi:10.1109/TPWRS.2020.2998579.
30. Rouzbehi, K.; Miranian, A.; Luna, A.; Rodriguez, P. Optimized control of multi-terminal DC GridsUsing particle swarm optimization. In Proceedings of the 2013 15th European Conference on Power Electronics and Applications (EPE), Lille, France, 3–5 September 2013; pp. 1–9. doi:10.1109/EPE.2013.6634326.
31. Namara, P.M.; Meere, R.; O'Donnell, T.; McLoone, S. Distributed MPC for Frequency Regulation in Multi-Terminal HVDC Grids. *IFAC Proc. Vol.* **2014**, *47*, 11141–11146. doi:10.3182/20140824-6-ZA-1003.01237.
32. Wen, Y.; Zhan, J.; Chung, C.Y.; Li, W. Frequency Stability Enhancement of Integrated AC/VSC-MTDC Systems With Massive Infeed of Offshore Wind Generation. *IEEE Trans. Power Syst.* **2018**, *33*, 5135–5146. doi:10.1109/TPWRS.2018.2792906.
33. Papangelis, L.; Debry, M.; Panciatici, P.; Van Cutsem, T. Coordinated Supervisory Control of Multi-Terminal HVDC Grids: A Model Predictive Control Approach. *IEEE Trans. Power Syst.* **2017**, *32*, 4673–4683. doi:10.1109/TPWRS.2017.2659781.
34. Raza, A.; Yousaf, Z.; Jamil, M.; Gilani, S.O.; Abbas, G.; Uzair, M.; Shaheen, S.; Benrabah, A.; Li, F. Multi-Objective Optimization of VSC Stations in Multi-Terminal VSC-HVdc Grids, Based on PSO. *IEEE Access* **2018**, *6*, 62995–63004. doi:10.1109/ACCESS.2018.2875972.
35. Gonzalez-Longatt, F.M.; Acosta, M.N.; Chamorro, H.R.; Torres, J.L.R. *Power Converters Dominated Power Systems*; Springer: Cham, Switzerland, 2021; pp. 1–35. doi:10.1007/978-3-030-54124-8_1.
36. COMMISSION REGULATION (EU) 2016/ 1447—of 26 August 2016—Establishing a Network Code on Requirements for Grid Connection of High Voltage Direct Current Systems and Direct Current-Connected Power Park Modules. p. 65. Available online: https://eur-lex.europa.eu/eli/reg/2016/1447/oj (accessed on 4 December 2020).
37. Saborío-Romano, O. Connection of OWPPs to HVDC Networks Using VSCs and Diode Rectifiers: An Overview. p. 5. Available online: https://www.researchgate.net/publication/322571208_Connection_of_OWPPs_to_HVDC_networks_using_VSCs_and_Diode_Rectifiers_an_Overview (accessed on 4 December 2020).
38. VDE/FNN. Technische Anschlussregeln für HGÜ-Systeme und über HGÜ-Systeme Angeschlossene Erzeugungsanlagen. Available online: https://www.vde.com/de/fnn/arbeitsgebiete/tar/tar-hgue (accessed on 4 December 2020).
39. Winter, W.; Chan, D.; Norton, M.; Haesen, E.; Székely, Á. Towards a european network code for HVDC connections and offshore wind integration. In Proceedings of the 2015 50th International Universities Power Engineering Conference (UPEC), Stoke on Trent, UK, 1–4 September 2015; pp. 1–6.
40. GmbH., T.T. Offshore-Netzanschlussregeln—O-NAR. 2017. Available online: https://docplayer.org/56149134-Offshore-netzanschlussregeln-o-nar-tennet-tso-gmbh.html (accessed on 4 December 2020).
41. Rate of Change of Frequency (RoCoF) Withstand Capability—ENTSO-E Guidance Document for National Implementation for Network Codes on Grid Connection. Available online: https://eepublicdownloads.entsoe.eu/clean-documents/Network%20codes%20documents/NC%20RfG/IGD_RoCoF_withstand_capability_final.pdf (accessed on 7 December 2020)
42. Need for Synthetic Inertia (SI) for Frequency Regulation—ENTSO-E Guidance Document for National Implementation for Network Codes on Grid Connection. Available online: https://eepublicdownloads.entsoe.eu/clean-documents/Network%20codes%20documents/NC%20RfG/IGD_Need_for_Synthetic_Inertia_final.pdf (accessed on 7 December 2020)

43. Chamorro, H.R.; Sanchez, A.C.; Verjordet, A.; Jimenez, F.; Gonzalez-Longatt, F.; Member, S.; Sood, V.K. Distributed Synthetic Inertia Control in Power Systems. In Proceedings of the 8th International Conference on Energy and Environment: Energy Saved Today is Asset for Future, CIEM 2017, Bucharest, Romania, 19–20 October 2017; pp. 74–78. doi:10.1109/CIEM.2017.8120874.
44. Chuquen, R.M.; Chamorro, H.R. *Graph Theory Applications to Deregulated Power Systems*; Springer Briefs in Electrical and Computer Engineering; Springer International Publishing: Berlin, Germany, 2021, doi:10.1007/978-3-030-57589-2.
45. Saad, H.; Peralta, J.; Dennetiere, S.; Mahseredjian, J.; Jatskevich, J.; Martinez, J.A.; Davoudi, A.; Saeedifard, M.; Sood, V.; Wang, X.; et al. Dynamic Averaged and Simplified Models for MMC-Based HVDC Transmission Systems. *IEEE Trans. Power Deliv.* **2013**, *28*, 1723–1730. doi:10.1109/TPWRD.2013.2251912.
46. Cole, S.; Beerten, J.; Belmans, R. Generalized Dynamic VSC MTDC Model for Power System Stability Studies. *IEEE Trans. Power Syst.* **2010**, *25*, 1655–1662. doi:10.1109/TPWRS.2010.2040846.
47. Haileselassie, T.M. *Control, Dynamics and Operation of Multi-terminal VSC-HVDC Transmission Systems*. 2012. Available online: https://ntnuopen.ntnu.no/ntnu-xmlui/handle/11250/257409 (accessed on 4 December 2020).
48. Fahad, S.; Mahdi, A.J.; Tang, W.H.; Huang, K.; Liu, Y. Particle Swarm Optimization Based DC-Link Voltage Control for Two Stage Grid Connected PV Inverter. In Proceedings of the 2018 International Conference on Power System Technology (POWERCON), Guangzhou, China, 6–8 November 2018; pp. 2233–2241.